Response of villin headpiece-capped gold nanoparticles to ultrafast laser heating

Hassan, Shabir ; Schade, Marco ; Shaw, Christopher P ; Lévy, Raphaël ; Hamm, Peter

Abstract: The integrity of a small model protein, the 36-residue villin headpiece HP36 attached to gold nanoparticles (AuNP) is examined and its response to laser excitation of the AuNPs is investigated. To that end, it is first verified by stationary IR and CD spectroscopy together with denaturation experiments that the folded structure of the protein is fully preserved when attached to the AuNP surface. It is then shown by time-resolved IR spectroscopy that the protein does not unfold even upon the highest pump fluences that lead to local temperature jumps in the order of 1000 K of the phonon system of the AuNPs, since that temperature jump persists for too short a time of a few nanoseconds only to be destructive. Judged from a blue shift of the amide I band, indicating destabilized or a few broken hydrogen bonds, the protein either swells, becomes more unstructured from the termini, and/or changes its degree of solvation. In any case, it recovers immediately after the excess energy dissipates into the bulk solvent. The process is entirely reversible for millions of laser shots without any indication of aggregation of the protein and/or the AuNPs and with only a minor fraction of broken protein-AuNP thiol-bonds. The work provides important cornerstones in designing laser pulse parameters for maximal heating with protein-capped AuNPs without destroying the capping layer.

DOI: https://doi.org/10.1021/jp500845f

Response of Villin Headpiece-Capped Gold Nanoparticles to Ultrafast Laser Heating

Shabir Hassan[1], Marco Schade[1], Christopher P Shaw[2], Raphaël Lévy[2], Peter Hamm[1]

[1]Department of Chemistry, University of Zurich, Zurich, Switzerland.

[2]Institute of Integrative Biology, University of Liverpool, Liverpool L69 7ZB, UK

Abstract: The integrity of a small model protein, the 36-residue villin headpiece HP36 attached to gold nanoparticles (AuNP) is examined and its response to laser excitation of the AuNPs is investigated. To that end, it is first verified by stationary IR and CD spectroscopy together with denaturation experiments that the folded structure of the protein is fully preserved when attached to the AuNP surface. It is then shown by time-resolved IR spectroscopy that the protein does not unfold even upon the highest pump fluences that lead to local temperature jumps in the order of 1000 K of the phonon system of the AuNPs, since that temperature jump persists for too short a time of a few nanoseconds only to be destructive. Judged from a blue shift of the amide I band, indicating destabilized or a few broken hydrogen bonds, the protein either swells, becomes more unstructured from the termini, and/or changes its degree of solvation. In any case, it recovers immediately after the excess energy dissipates into the bulk solvent. The process is entirely reversible for millions of laser shots without any indication of aggregation of the protein and/or the AuNPs and with only a minor fraction of broken protein-AuNP thiol-bonds. The work provides important cornerstones in designing laser pulse parameters for maximal heating with protein-capped AuNPs without destroying the capping layer.

Keywords: Villin Headpiece 36 (HP36), gold nanoparticles (AuNP), amide I, laser heating.

Introduction

Nanomaterial-based carriers have provided a novel and effective route for targeted drug delivery[1] as well as cancer treatment and diagnosis.[2-8] Over the last decade, various delivery vehicles have been designed based on different nanomaterials, such as liposomes[1,9], dendrimers,[10] nanotubes[11] and nanorods.[12] Recently, gold nanoparticles (AuNPs) have also emerged as a candidate of choice for targeted delivery of drugs[13] and various biomolecules.[14] There are many ways to control sustained release of drugs within the therapeutic window from AuNPs used as drug delivery systems, such as by the biocatalytic action of an enzyme,[15,16] differential concentration of intracellular glutathione versus extracellular thiol levels,[17,18] photothermal or photodynamic therapy,[8,19-21] etc. AuNPs with antibodies on the surface that specifically bind to cancer cells are significantly more efficient; otherwise phototherapy would not be selective and would affect normal and tumor cells alike.[22] For the latter applications, it is critical to understand the folding and stability of biomacromolecules on AuNPs under the influence of laser radiation.

Most attention, so far, has been given to the cell fate in response to applied laser intensities. In contrast, the effect on the capping molecules of AuNPs used in photothermal and photodynamic treatments has barely been studied. Apart from a few reports on the heating effects on DNA and bovine serum albumin (BSA) conjugated with AuNPs,[23-25] basically nothing is known about the dynamics or structural changes of a protein or an antibody attached to the AuNP surface upon heating by a laser beam. Heat absorbed by the AuNPs is transferred to the biomolecule and the local environment by rapid electron-phonon relaxation in the AuNP followed by phonon-phonon relaxation,[26-28] resulting in an increase in the temperature of the surrounding medium.[29] Under such conditions, an important question is whether the attached protein remains stable, and if yes, up to which laser intensities? It has been shown that AuNPs can reach dramatic temperatures upon pulsed laser excitation[30] reaching many hundreds of degrees Celsius, that in principle would unfold any protein on the surface of a AuNP or dissociate the covalent bond between protein and AuNP. On the other hand, heat deposited into a AuNP dissipates very quickly into the bulk solution within a few 100 ps[25], many orders of magnitude faster than typical protein unfolding times.[31] On the other hand, the temperature jump is quite moderate after thermalization into the bulk solution (in the order of 1 K for the excitations conditions discussed in this paper), *per se* too small to unfold a protein. The interplay between the size of the initial temperature jump and its short lifetime will determine whether a protein actually unfolds. If it does unfold, it might be irreversible and lead to aggregation of the protein and/or the AuNPs.

Independent from the question about the stability of conjugated proteins, local heating is also interesting as a method to study vibrational energy transport in molecular systems. This idea has been explored for example for thiolated self-assembled monolayers (SAMs) of aryl and alkyl thiol adsorbates on a polycrystalline Au (111) surface[32,33] or for a helical peptide layer on small AuNPs.[34] These works address the question whether heat transport is ballistic[32,33] diffusive[34], and, ultimately, whether vibrational energy transport is isotropic or can occur through defined pathways. Directed vibrational energy transport is discussed as a possible mechanism of communication in allosteric proteins.[35]

In the present work, we examine the integrity of a small model protein, the 36-residue villin headpiece HP36, attached to AuNPs and investigate its response to the deposited laser energy. A sketch of the system under study is shown in Figure 1. HP36 has been used extensively to study protein folding, both experimentally and theoretically.[36-46] Because of its monomeric nature, high thermal stability, and the fact that it shows properties of a folded protein despite its small size, the thermodynamics of HP36, its folding kinetics, and

structural dynamics, etc., have been fully characterized and it therefore constitutes an interesting model system.[36-46] To the best of our knowledge, there is however no report on the effect on secondary and tertiary structure of HP36 when attached on a AuNP. We report on the synthesis and characterization of HP36/AuNP conjugates and we look into the dynamic response of the protein upon pulsed laser irradiation of the AuNP.

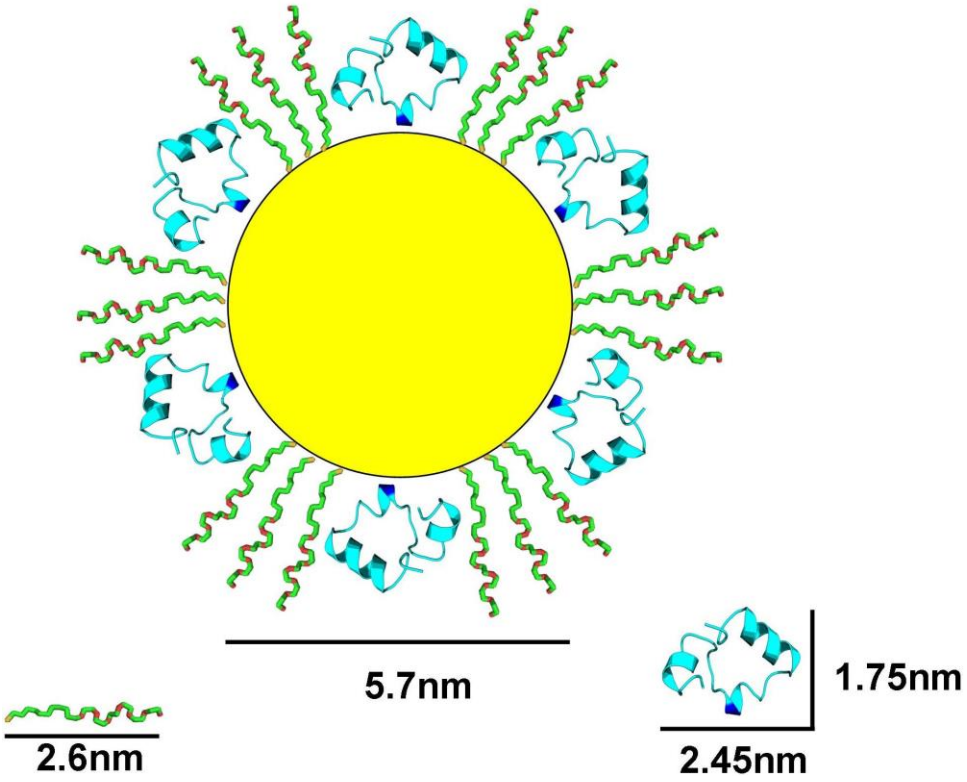

Figure 1: Sketch to the scale of HP36Cys (cyan) attached to AuNPs of 5.7 nm diameter (yellow) through a cysteine residue. PEG molecules (green) are shown in a stretched configuration.

Materials and Methods

Protein Synthesis

The wild-type villin headpiece HP36WT (PDB ID: 1VII) has no thiol containing amino acids that could be attached to a AuNP surface. Therefore, Serine at position 56 was replaced by Cysteine – resulting in the mutant HP36Cys – to provide a specific anchor point (in line with previous studies of HP36, the numbering of amino acid residues is based on the full-length 76 residue villin headpiece with the first residue of HP36 assigned to position 41). This position was chosen because it is solvent exposed and thus easily accessible to the linking reaction.

HP36 and HP36Cys samples were synthesized in-house on a peptide synthesizer (CEM) using the standard solid-phase Fmoc protection protocol with Rink Amide MBHA resin (100-200 mesh, 0.1-0.25mmol) to achieve a stepwise coupling of amino acids. All the chemicals were bought from Sigma Aldrich and used as received. The crude samples were

purified using a Cosmosil $5C_4$ HPLC column with a 30%-80% acetonitrile:water gradient in presence of 0.1% trifluoroacetic acid (TFA). The samples were dried *in vacuo* and analyzed with electro spray ionization mass spectrometry (Figure S1). Purity of the protein was about 85%.

AuNP Synthesis and Functionalization

Tannic acid capped AuNPs were synthesized as reported earlier.[47] In brief, for a 100 ml reaction, 1 ml of 1% w/v $HAuCl_4$ was added to 79 ml of MilliQ water (18.2 MΩ·cm) and heated to 60°C. While the gold solution was heating, a reducing solution of 4 ml 1% w/v of tri-sodium citrate dehydrate ($Na_3C_6H_5O_7.2H_2O$) and 1 ml 1% w/v of tannic acid in 14 ml MilliQ water was prepared and put in a water bath maintained at 60°C. Just before adding the two solutions together for the reduction reaction, 1 ml 0.2M K_2CO_3 was added to the gold solution, followed by quickly adding the reducing solution. As soon as the second solution was added, the yellow gold solution turned to red wine color, characteristic for AuNP formation. The solution was refluxed at 95°C for half an hour, cooled down and filtered through a 0.45 μm syringe filter before storing at 4°C.

For transmission electron microscope (TEM) measurements, the AuNPs were applied to a previously glow discharged, carbon-coated 300 mesh copper grids for 1 min; the excess solution was immediately blotted dry with filter paper. Microscopy was performed with a Philips CM100 TEM operating at an accelerating voltage of 80 kV. High-resolution TEM images were captured with a fitted 4k×3k pixel 12-bit Gatan digital camera and processed using the Image J and Origin program packages. Figure S2 shows a TEM image together with a size distribution, revealing an average diameter of 5.7±1nm and a polydispersity of 21%.

For the functionalization of the AuNPs, a 5:1 molar mixture of thiolated PEG ($SHC_{11}EG_6OH$, hereafter named PEG) and HP36Cys was used. The reaction was carried out overnight in the presence of a detergent (3 mM SDS). To avoid oxidation of the PEG molecules into aldehydes and carboxylate salts (visible through the asymmetric carboxylate stretch peaking at 1605 cm^{-1} in the FTIR spectrum), PEG samples were freshly prepared in ethanol and all the chemical solutions, including AuNPs, were degassed for 2 hours before functionalization in a nitrogen purged environment.

Filtration and Desalting

Excess tannic acid, PEG and SDS as well as unreacted protein molecules were filtered out using a 30 kDa centrifugal cut-off filter (Amicon filters from Milipore). The conjugate was then run through a FPLC desalting column (GE Healthcare HiPrep 26/10). In order to prevent aggregation of the protein-AuNP conjugate on the column, it was saturated with 100 μM SDS in deionized-degassed water before applying the samples. The concentration of SDS was chosen such that it was enough to prevent aggregation but well below the critical micelle concentration (8 mM). The filtrate was concentrated and lyophilized for later D_2O exchange required for the IR spectroscopy

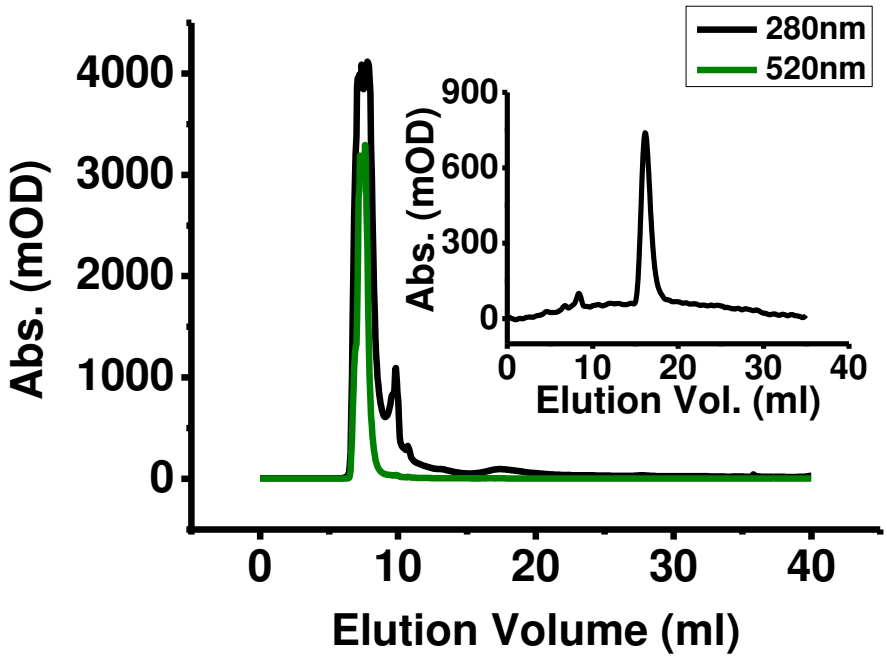

Figure 2: FPLC chromatogram of the HP36/AuNP conjugate at 520 nm (green) and 280 nm (black). Inset: FPLC of tannic acid in water at 280 nm.

Figure 2 depicts a chromatogram of the filtered protein-AuNP conjugates measured at 520 nm (green, sensitive to the surface plasmon resonance of the AuNP) and 280 nm (black, sensitive to the protein as well as to tannic acid). At both wavelengths, a first peak at around 7.5 ml elution volume from the HP36/AuNP conjugate is observed, followed by two more peaks appearing at 9 ml and 18 ml observed only at 280 nm. Figure 2 (inset) shows an independent chromatogram for tannic acid in water, showing that the 18 ml stems from residual tannic acid, thus the 9 ml peak in Figure 2 stems from unbound proteins. The 7.5 ml elution peak was therefore collected as the final purified sample. It contains only minor contributions from unbound protein (<10%).

Laser Setup

The response of the amide I vibration of the proteins attached to the AuNPs was measured by UV pump/IR probe spectroscopy. Laser pulses from a Ti:sapphire laser/amplifier system (repetition rate 1 kHz) were split into two parts. One portion was frequency doubled in a BBO crystal generating 400 nm pulses of 100 fs duration. This pump beam was mechanically chopped at half the laser repetition rate and used for the excitation of the protein-AuNPs conjugates. The diameter of the 400 nm pump beam at the sample was 150 µm. The pump fluence at the sample was varied with the help of an adjustable neutral density filter from ≈20 J/m^2 to 110 J/m^2.

The second part was used to feed a white light-seeded two-stage optical parametric amplifier (OPA)[48] for the generation of infrared probe pulses (center frequency 1650 cm^{-1}, bandwidth 200 cm^{-1}). The probe pulses were focused into the sample in spatial overlap with the pump pulses; a reference beam, split off beforehand, was focused about 1 mm separated into a non-excited volume of the sample. Both probe and reference beams were frequency dispersed in a spectrometer and imaged onto a double-array HgCdTe detector with a spectral resolution of ≈4 cm^{-1}. The pump pulse was delayed with respect to the probe

pulse with the help of an optical delay stage. The overall instrument response time was 200 fs.

The protein-AuNPs conjugates were dissolved in D_2O at with a concentration of proteins of ≈2 mM and measured in an optical cell with path length 50 μm. The samples were stable over millions of laser shots and no flow cell to exchange the sample volume between laser shots was necessary.

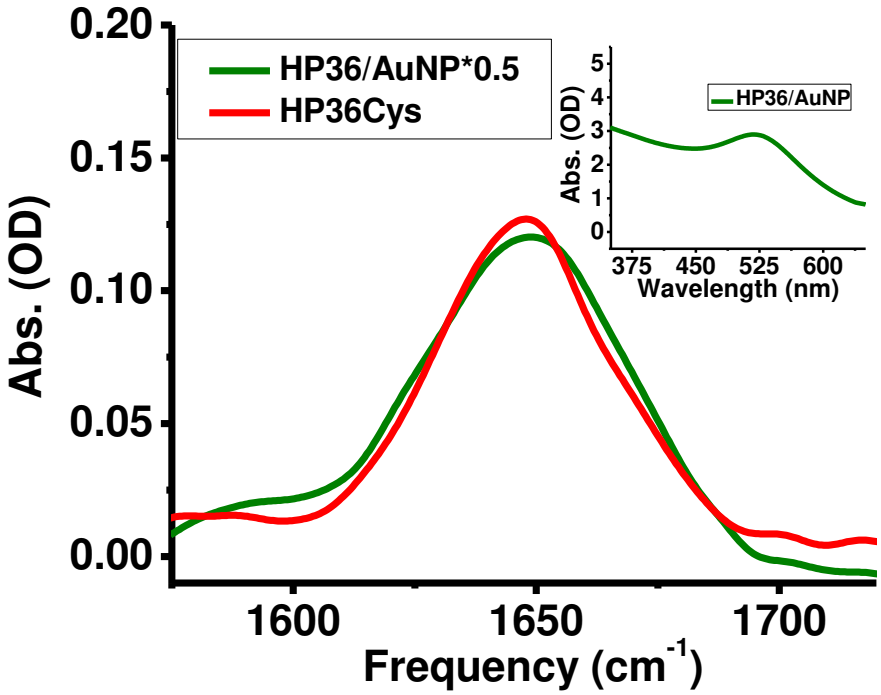

Figure 3: FTIR spectra of free HP36Cys (red) and of HP36/AuNP (green) in the amide I region and (inset) UV-Vis spectrum of HP36/AuNP.

Results: Structural Characterization

UV/VIS and FTIR Spectroscopy

The UV-Vis spectrum was measured to see to what extent functionalization and the subsequent cleaning process affects the stability of the AuNPs (Figure 3, inset). A clear surface plasmon resonance peak at 520 nm without any additional feature or shift suggests that the AuNPs are indeed stable.

Apart from revealing characteristic absorption peaks for alpha helices, beta-sheets and random coils, Fourier transform infrared (FTIR) spectroscopy also gives a first hand look into aggregation of the proteins into amyloids/beta-sheets, in which case a distinct absorption band at 1618 cm^{-1} and a minor component at the high-frequency end of the amide I region would be observed.[49] FTIR spectroscopy was therefore performed as a first step to investigate the protein stability upon conjugation with AuNPs. Figure 3 shows the FTIR spectra of HP36Cys (red) and HP36/AuNP (green), both redispersed in D_2O at concentrations ≈2 mM and ≈4 mM protein, respectively (both spectra in Figure 3 have been scaled accordingly to the same intensity). Both samples show a broad amide I band centered at ≈1645 cm^{-1}, as is expected for an α-helical protein in D_2O.[49] The absence of a

characteristic amyloid aggregation signature shows that the conjugate is stable even at the high concentrations needed for IR experiments.

The attached PEG molecules do not interfere with amide I spectrum, as their absorption is flat between 1550 cm^{-1} and 1750 cm^{-1} (see Figure S3). The intensity of the 1100 cm^{-1} peak, characteristic for the ether group of PEG, would correspond to ≈30 mM PEG concentration, about eight times more than that of protein. The characteristic peak for tannic acid (1600 cm^{-1}, see Figure S3), is missing from the FTIR spectra of HP36/AuNP, confirming complete exchange during functionalization.

At this point it is however important to note that the concentrations of protein and PEG in the HP36/AuNP sample given above (4 mM and 30 mM, respectively) were determined by comparing the intensities of their IR absorption spectra with those of PEG and HP36Cys in solution. This procedure implicitly assumes that the IR cross section is the same in solution and on the AuNP surface, which is known not to be correct. Surface enhancement effects can modify the cross section by a factor 1.5-5, depending on the AuNP radius, distance from the surface and orientation relative to the surface.[50-53] In certain cases, surface selection rules can also decrease the cross section, but when averaging over individual amide I vibrations with all possible orientations, as in a globular protein, the overall cross section will always be enhanced. AuNPs of size 5.7 nm have a surface area of ≈100 nm^2, while cross-sectional areas of ≈3 nm^2 for the protein (Figure 1) and 0.2 nm^2 for PEG would require ≈200 nm^2 if the concentrations given above were correct. We therefore conclude that surface enhancement effects overestimate the concentrations by roughly a factor 2. Taking all together, the sum formula of the protein-AuNP conjugate is thus roughly $Au_{5700}PEG_{200}Protein_{25}$. It should be added though that the above estimate assumes that PEG is in an extended conformation, which is not necessarily the case. As such, the enhancement factor is considered to be a lower limit and the resulting number of PEG molecules on the AuNPs an upper limit.

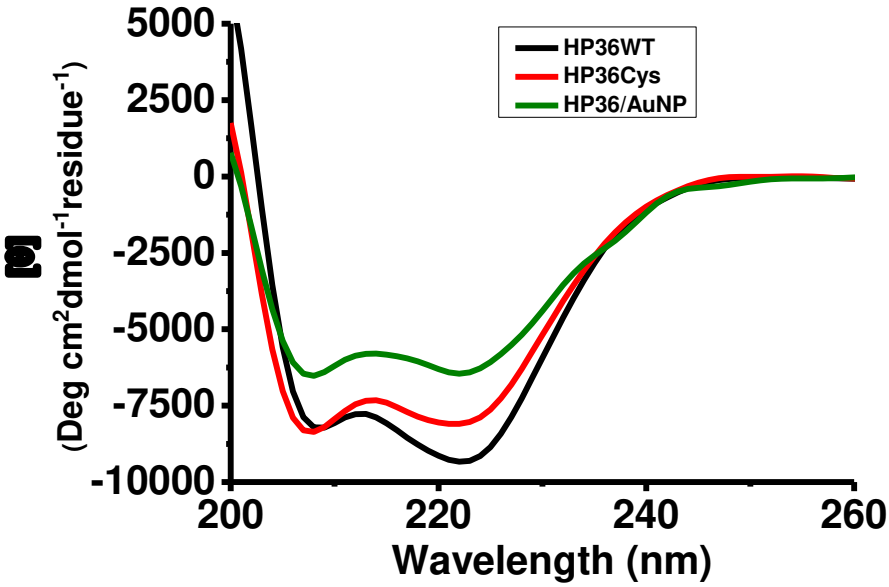

Figure 4: CD spectra expressed in terms of the mean residue ellipticity (MRE) of HP36WT (black), HP36Cys (red), HP36/AuNP conjugate (green).

CD Spectroscopy

Circular dichroism (CD) spectroscopy is a sensitive probe of, in particular, α-helices, which is the dominant secondary structure motif of HP36. CD spectra were recorded at 25^0 C with the help of a Jasco Spectropolarimeter (Model J-810) in a 10 mm path length quartz cuvette. Purifying the conjugate from any unreacted proteins by FPLC (Figure 2) ensured that we selectively study the folding of proteins attached to the AuNP surface**.** CD spectroscopy of ligands attached to AuNPs is challenging because the metal core strongly absorbs in the far UV. Therefore, the best compromise between CD signal-size and background absorption was searched in terms of signal-to-noise ratio, resulting in a concentration of ≈4 μM with an absorbance of A≈2 at 222 nm. Spectra were averaged over ≈1000 scans to increase the signal-to-noise ratio. The AuNP contribution to the CD signal, which has been measured independently, has been subtracted (but, as expected, its contribution was minor).

Figure 4 shows CD spectra of HP36WT, HP36Cys (to assess the effect of the mutation on the stability) and HP36/AuNP. The two characteristic peaks at 208 nm and 222 nm are indicative for a helical structure, which is very similar for both the wild type protein HP36WT and the mutant HP36Cys. In the case of the conjugate HP36/AuNP, the shape of the CD signal remains the same, clearly indicating that the protein is still α-helical on the AuNP surface. It should be added that the amplitude of the CD signal in Figure 4 requires the knowledge of protein concentration, which has been estimated from the IR absorption together with a surface enhancement factor of ≈2 discussed above. At the same time, this analysis assumes that surface enhancement effects play essentially no role for the CD signal (which to the best of our knowledge have not been investigated as of yet).

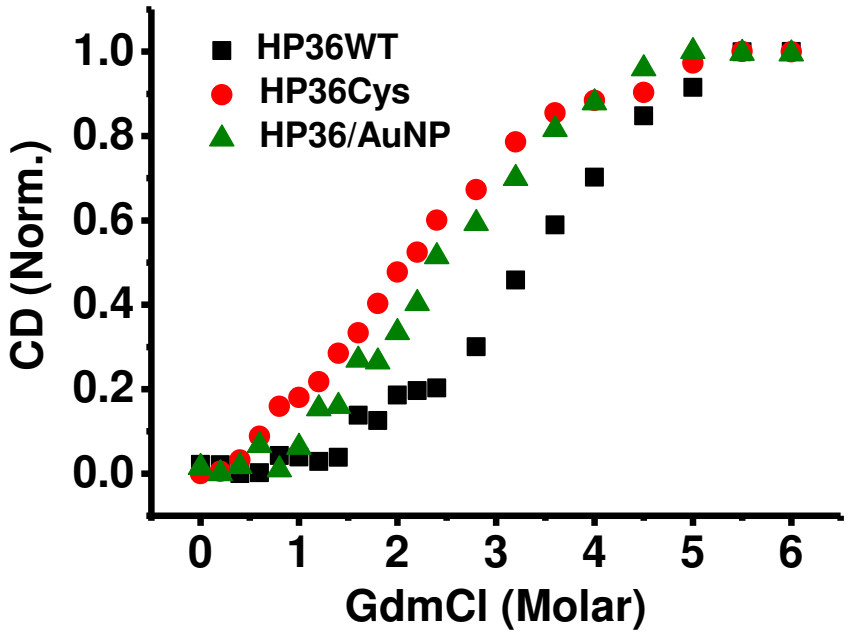

Figure 5: Unfolding of HP36WT (black), HP36Cys (red) and HP36/AuNP (green) upon addition of guanidinium. The CD signal at 222nm was measured as a function of varying concentration of guanidinium chloride at 25°C and normalized for comparison.

To further probe the folding of the protein, we performed denaturation experiments for all three samples as a function of guanidinium concentration (Figure 5), again at 25°C. From the mid-points of these unfolding curves we see that mutant HP36Cys (2.1 M) is slightly less stable than the wild type HP36WT (3.2 M). Furthermore HP36/AuNP goes through a characteristic sigmoidal unfolding transition with a mid-point that is the same as HP36Cys. From the plateau of that sigmoidal transition at low guanidinium concentrations, we conclude again that HP36/AuNP is folded on the AuNP surface, and that the AuNP surface does not affect its stability.

Results: Heat Response

Laser excitation of the AuNP leads to a rapid temperature jump within the AuNP on a picosecond time scale through electron-phonon relaxation followed by phonon-phonon scattering.[27,28,54] That temperature jump eventually also affects the capping layer. To study the response of HP36, HP36/AuNP was excited with a 400 nm laser pulse and time resolved infrared spectra were recorded in the amide I region (i.e. the C=O stretch vibration of the protein backbone). The spectral window considered here is free from vibrational bands of the other capping molecule, PEG (Figure S3). On the other hand, the contribution of electrons in the conduction band of the metal core at early delay times as well as the heating of the bulk solution at later delay times cause a tilted broadband background that was removed from the transient spectra by subtracting off a linear baseline determined from the edges of the detected spectral window.

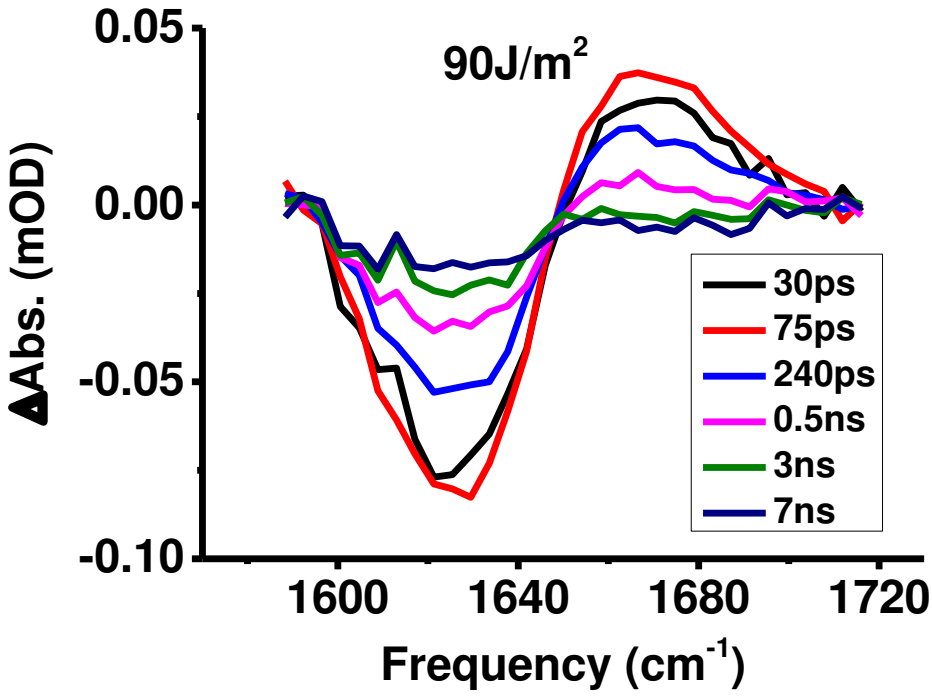

Figure 6: Pump-probe spectra of the amide I band recorded at various delay times (black 30 ps, red,75 ps, blue 240 ps, magenta 0.5 ns, green 3 ns, dark blue 7 ns) after laser excitation of the AuNP with a pump fluence of 90 J/m².

A time series of pump-probe difference spectra is shown in Figure 6. The absorption decreases on the red side of the amide I absorption spectrum (see Figure 3) and increases on the blue side; that is, the response in Figure 6 reflects a blueshift of the protein amide I

band. Apart from the overall intensity of the signal, the spectral response is the same at all delay times within signal-to-noise.

Figure 7 shows the time-dependence of the transient signal for different pump fluences (the difference between the negative feature at 1625 cm^{-1} and the positive feature at 1666 cm^{-1} is shown in order to be as insensitive as possible to residual backgrounds from conducting electron or solvent heating effects). The signal peaks at 75 ps and then decays on a few nanosecond timescale. Normalizing all curves onto each other (Figure 7, inset) shows that the kinetics of the amide I band response do not change with pump fluence within signal-to-noise (the outliers in that plot stem from the data with very low pump-energy, which consequently become rather noisy).

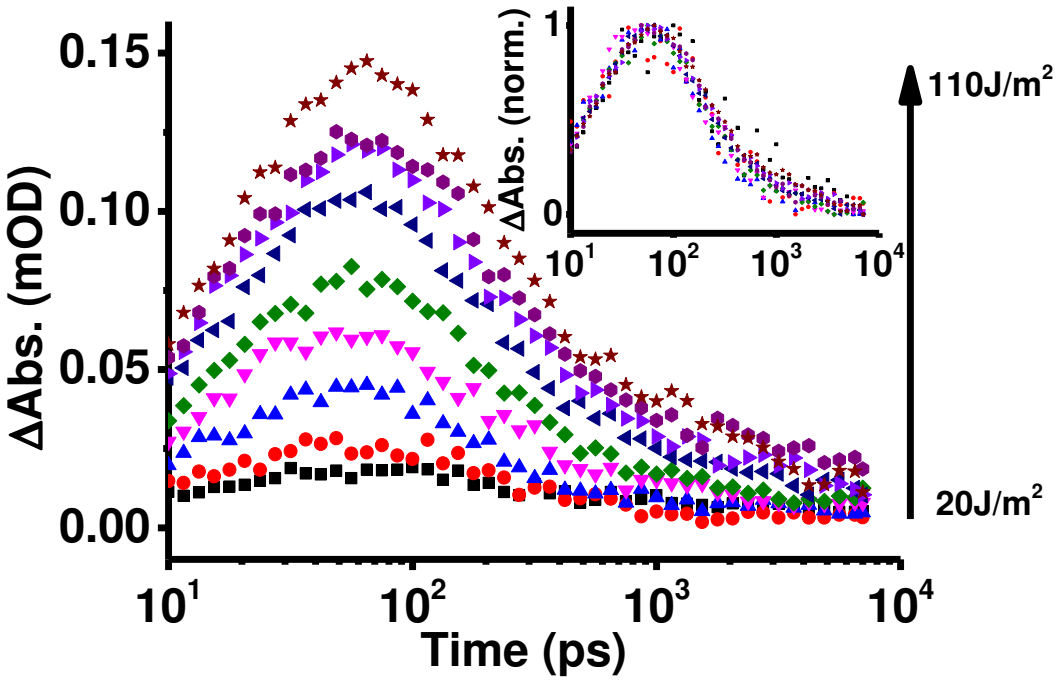

Figure 7: Time dependence of the blue shift (calculated as the difference between the negative and positive spectral feature) recorded for the pump fluence varied from 20 J/m² to 110 J/m². The inset shows the same curves normalized onto each other.

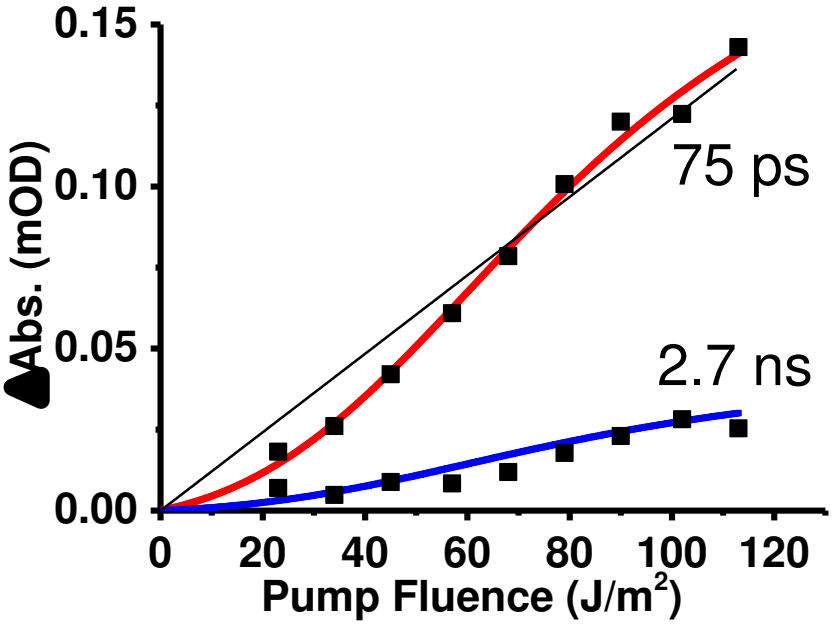

Figure 8: Amplitude of the transient signal (calculated as the difference between the negative and positive spectral feature) as a function of pump fluence, evaluated at the peak of the signal (75 ps) and towards the end of the process (2.7 ns). The thick red and blue lines are fits of Eq. 1 to the data, the thin black line the best linear fit. See text for discussion.

In Figure 8 we show the peak amplitude of the transient signal as a function of pump fluence evaluated at 75 ps and at 2.7 ns, respectively. Interestingly, the protein response upon AuNP heating is not linear. The thin black line in Figure 8 shows the best linear fit to the 75 ps data, when forcing it to go through the origin, which it should since no signal is expected without pump. The linear fit systematically deviates from the data. In contrast, a fit based on a two-state equilibrium (Eq. 1 discussed below) perfectly reproduces the sigmoidal shape of the response (thick red line) with root-mean-square-displacement (rmsd) that is improved by a factor 3. The same model parameters (except for a smaller amplitude) also fit the late 2.7 ns data (thick blue line).

Finally, we note that the process is completely reversible and the proteins remain unchanged over millions of laser-induced heating-cooling cycles. Figure S4 shows that the pump-probe signal decreases by only about 10% in intensity for 90 J/m^2 pump fluence within ≈75 min of measurement time, corresponding to $2.3 \cdot 10^6$ pump laser shots hitting the sample. Only a minor fraction of the gold-protein thiol bonds is thus dissociating. The sample was not actively exchanged during that measurment time by flowing the sample, stirring, or moving the sample cell, but a certain exchange due to diffusion certainly happened. Furthermore, the shape of the amide I response remains the same, indicating that no aggregation nor irreversible unfolding of the protein took place.

Discussion

Structural Characterization

AuNPs have been shown to bring about a change in stability and structural properties of many proteins attached to their surfaces.[52,55-57] For example in Ref.[52] it has been shown that a peptide (CFGAILSS) prone to aggregate into extended amyloid fibrils with an antiparallel β-sheet structure in aqueous solutions, when constrained to a nanoparticle surface, it has a curvature-dependent tendency to form parallel β-sheets with hydrogen bonding between adjacent peptides. Another example is small AuNPs capped by cytochrome C, which revealed local perturbation and considerable denaturation of the α-helical part of the protein.[55]

In contrast to these previous works, we provide here multiple evidences that the villin headpiece HP36 does in fact stay stably folded on the AuNP surface. That is, the IR absorption spectrum does not give any indications of aggregation (Figure 3) and we observe the characteristic CD spectrum of a helical protein with two negative peaks at 222 nm and 208 nm. In addition, the sigmoidal response upon guanidinium denaturation reveals a distinct transition at about the same denaturant concentration as the HP36Cys mutant (Figure 5), hence the AuNP surface has essentially no effect on the stability of the protein (while the Serine to Cysteine mutation has a sizeable effect). The explanation for this high stability of the conjugated protein may lie in large number of PEG molecules that surround the protein in the ligand layer: at least in solution, PEG has been shown to stabilize the secondary structures of α-helical peptides by reducing the solvent accessible surface area.[58]

The structural picture that emerges from the stationary characterization of the protein-AuNP conjugates is sketched in Figure 1 with an overall sum formula of the protein-AuNP conjugate of approximately $Au_{5700}PEG_{200}Protein_{25}$. The sketch is on scale, but it assumes that the PEG molecules adopt a stretched configuration, which probably does not reflect the reality. On the other hand, we know from CD spectroscopy that the proteins are stably folded. We therefore assume that the proteins are mostly surrounded by PEG, with only small direct contact to the solvent water.

Heat Response

Laser excitation of the AuNPs at 400 nm excites the electronic system of the AuNPs, which relaxes via electron-phonon coupling into the phonon system.[26-28,30,54] For our experimental conditions, we can estimate from the absorption cross section and the heat capacity of gold that every AuNP absorbs approximately 500 photons (assuming an extinction coefficient of $1.3 \cdot 10^7$ $M^{-1}cm^{-1}$, which was linearly interpolated for the 5.7 nm AuNPs from the values given in Ref.[59] and corrected for the fact that we excited at 400 nm and not in the Plasmon resonance), resulting in an initial temperature jump of 1000±200 K at the highest pump fluence we considered, 110 J/m^2. This estimate of the temperature jump is consistent with previous works.[30] It is important to realize that in contrast to molecular heaters,[60] which either absorb a photon or not, AuNPs can absorb many photons for a single laser shot. Hence, the pump fluence determines the size of the initial temperature jump, and not the probability with which an individual molecule is excited.

The phonon system subsequently cools into the environment, i.e. into the capping layer and eventually into the solvent. It has been shown that the timescale on which the AuNP cools is a function of particle size.[27] It scales roughly as the square of the AuNP radius, which reflects the solution of a diffusion equation together with the surface/volume ratio of a spherical particle. For 5.7 nm particles used here, a cooling time of 10±5 ps has been

reported.[27] That value has been measured for AuNPs in water without capping layer, but what enters in the theory is the thermal conductivity of the surrounding of the AuNP, that is not very different for our capping layer,[61] so the cooling time of the AuNPs *per se* is of the same order of magnitude. It has been shown (albeit for smaller temperature jumps)[27] that the cooling time is not a function of the size of the temperature jump.

Due to the interfacial thermal resistance at the AuNP surface, the temperature jump reached in the capping layer is significantly smaller than that in the AuNP itself, and the heat transfer is delayed. For example, Plech and coworkers have shown that the water layer in contact with 10 nm AuNPs reaches a maximum temperature jump of only 30% of that of the AuNP, and that this maximum temperature is reached after 150 ps.[25] Given that our AuNPs are smaller (5.7 nm), we conclude that the peak maximum we observe in the amide I response (75 ps, see Figure 7) reflects the time when the temperature in the protein capping layer is maximal. Ref. [25] investigated the heat transfer from a AuNP directly into the solvent, whereas the proteins in our case are covalently bound, so the interfacial thermal resistance might be smaller,[62] and consequently the heat jump might be somewhat larger than the 300 K that would be estimated along the lines of Ref. [25].

A temperature jump in that order of magnitude, of course, would unfold any protein (for our particular case, the melting temperature of HP36WT is 71°C[36]). Furthermore, it could result in a barrier-free unfolding, in which case it might become must faster than known protein unfolding times. Indeed, the shape of the blue-shifted amide I response (Figure 6) is qualitatively the same as that observed in a stationary thermal unfolding experiments of the villin headpiece.[44-46] But if the protein would really unfold, its refolding, which could occur only once the system has cooled completely into the bulk solvent, would occur with the typical few microsecond folding time of HP36.[31,43] In contrast, we observe that the amide I signal recovers on a nanosecond timescale (Figure 7), orders of magnitudes too fast to account for a refolding kinetics. On the other hand, the timescale of the recovery of the amide I signal we observe agrees well with what is predicted from radial heat diffusion from the AuNPs into the bulk solvent.[25] Hence, the protein is not unfolding upon the temperature jump, because the temperature jump exists for too short a time to be destructive. In accordance with that conclusion, the size of the signal in Figure 6 is indeed significantly smaller than one is obtained in a thermal unfolding experiment.[44,45]

The absorption frequency of the amide I vibration red-shifts by ≈20 cm^{-1} upon hydrogen bonding,[49] hence, the blue-shift we observe after the temperature jump (Figure 6) reflects an overall weakening of either the intramolecular hydrogen bonds of the protein or of those to water around the protein. Breaking of intramolecular hydrogen bonds is the very reason why a similar blueshift is also observed upon thermal unfolding of the villin headpiece,[44-46] but, as discussed above, that cannot be what is happening here. Also *N*-methyl- acetamide (NMA) with only one amide unit and no structural flexibility undergoes spectral shifts due to weakening of hydrogen bonding to the solvent.[63] We assume that the proteins are either swelling thereby increasing in average all hydrogen-bond distances, destabilizes from the termini, and/or changes with respect to its solvation shell. Whatever the process is, it does however not yet lead to any irreversible structural change that would destroy secondary or tertiary structural motifs. The protein can thus restore its original structure essentially instantaneously once the system cools back to room temperature. A vibrational Stark effect, that has also been shown to cause shifts in the amide I spectrum[64] can be excluded as its kinetics would follow the much shorter lifetime of the electronic excitation of the AuNP.

An interesting observation is the nonlinear dependence of the protein response on pump fluence (Figure 8). The sigmoidal shape suggests some degree of cooperativity of the

process. Without any concrete molecular dynamics simulation of the system, our discussion of that effect will remain rather vague and speculative. It is nevertheless intriguing that the experimental data ΔA can be fit to a simple two-state chemical equilibrium (where we implicitly assume that the system reaches a quasi-equilibrium on the timescale of the experiment):

$$\Delta A(\Delta T) \propto \frac{1}{1+e^{\frac{\Delta F}{k_B(T_0+\Delta T)}}} - \frac{1}{1+e^{\frac{\Delta F}{k_B T_0}}} \qquad (1)$$

Here, T_0 is the starting temperature (i.e., room temperature), ΔT is the temperature jump in dependence of the pump fluence, $\Delta F=\Delta E-T\Delta S$ is a free energy with $T=T_0+\Delta T$, and the second term assures that the response ΔA is zero for $\Delta T=0$. The fit shown in Figure 8 (red line) reveals an energetic contribution of ΔE=23 kJ/mol and an entropic contribution ΔS=45 J/(mol·K), the latter of which must reflect the entropy gain of the destabilized protein. These numbers assume that the temperature jump of the protein is 300 K at a pump fluence of 110 J/m^2; if the temperature jump is larger due to an interfacial thermal resistance that is smaller than what is assumed in Ref.[25] (see discussion above), then ΔE and ΔS would be correspondingly smaller. In any case, the energetic contribution ΔE=23 kJ/mol is in the range of the typical binding energy of one hydrogen bond, so the analysis gives an idea on the amount of structural modification in the transiently destabilized state.

The process is almost completely reversible and the protein-AuNP conjugates remain essentially unchanged over millions of laser-induced heating-cooling cycles. First, only a small fraction (≈10%) of the AuNP-protein thiol-bonds break after about 2.3*10^6 laser shots. A roughly quadratic energy dependence of thiol-bond cleavage of AuNP-ligand conjugates has been observed in Ref.[24] with a cleavage efficiency of 4*10^{-4} for 3 μJ pulses focused onto a 100 μm spot, using comparable pulses at 400 nm with 100 fs duration. This number is in qualitative agreement with our observation, given the fact that our pump fluences are lower (the values reported in Ref.[24] correspond to 400 J/m^2 pump fluence) and that a certain diffusive exchange of sample into and out from the pumped volume does occur during the measurement (which prevents us from quantifying the cleavage efficiency).

Second, the proteins remain folded without any sign of aggregation. The high stability of our system can be attributed to the high intrinsic stability of HP36 combined with the refolding capabilities of PEG which is present at a very high local concentration. Indeed several studies have shown that high concentration of PEG enable the refolding of proteins either through molecular interactions ("chaperon" type effect)[65] or through molecular crowding.[66]

Conclusion

In this study we report on the stability of the villin headpiece 36 (HP36) attached to small AuNPs. From IR and CD spectroscopy together with denaturation experiments we conclude that the AuNP surface does essentially not affect the stability of the protein, a result which we attribute to the high intrinsic stability of HP36 as well as the high PEG content of the capping layer. Even more so, the protein still stays stable upon laser pumping of the AuNPs that reach dramatic temperatures jumps up to 1000 K. Even though the temperature jump of the protein is presumably significantly smaller due to the interfacial thermal resistance, it is still large enough to, in principle, unfold any protein. However, the temperature jump

persists for too short time of a few nanoseconds only to be destructive. Consequently, the protein swells or becomes a bit unstructured from the termini, as indicated by destabilized or broken intramolecular or solvent hydrogen bonds, but not yet to the extent that tertiary or secondary structure is destroyed, so the original folded structure of the protein is restored essentially instantaneously once the excess energy dissipates into the bulk solution. The process is entirely reversible for millions of laser shots with only minor cleavage of the protein-AuNP thiol-bonds and no indication of an aggregation of the protein and/or the AuNPs. It would be very interesting to address the question what the structure of the transiently destabilized state is by molecular dynamics (MD) simulations. In terms of system size and required simulation length, such MD simulations would be well within reach, and models that relate structures from a MD trajectory to the amide I spectrum are well developed.[46]

The study provides important cornerstones for the design of protein-AuNP conjugates as well as of the excitation scheme for phototherapeutic purposes. That is, we address the interplay of the size of the temperature jump on the one hand *versus* its short lifetime on the other hand, and show that a protein may remain stably folded even at pretty large pump fluences. Villin headpiece is a small and as such a fast folding protein.[31,43] We have shown that the folded state on the AuNPs is kinetically stabilized after the heat jump. One may therefore assume that larger proteins with corresponding even longer folding times survive such a short-lived temperature jump equally well.

We considered a pulsed excitation here, while cw-excitation is more common in concrete applications. The nonlinear response (Figure 8) emphasizes that pulsed or cw-excitation may result in a qualitatively different mechanism. cw-Excitation integrates over the heating-cooling response shown in Figure 7, which for typical intensities (50 W/cm^2)[67] would correspond to a pulsed excitation with 0.5 mJ/m^2 (assuming an integration time of 1 ns), orders of magnitudes lower than what is used in the present study. But the heat jump then is stationary, and affects the bulk solution as well, so it might be destructive despite the fact that it is much smaller. In terms of the amount of energy that can be deposited into a cancer cell without directly destroying the protein-AuNP conjugates, pulsed excitation with an optimal compromise between laser repetition rate and pulse energy might therefore be advantageous.

Acknowledgement

We thank Martin Volk (Liverpool) for a critical reading of the manuscript and very valuable comments, Rolf Pfister (University of Zurich) for his help with the synthesis of HP36WT and HP36Cys, Bernard Spingler (University of Zurich) for providing access to the CD spectrometer, the Centre for Microscopy and Image Analysis (University of Zurich) for access to the TEM facility, the Functional Genomics Centre (University of Zurich) for help with mass spectrometry, and Jan Helbing and Paul Donaldson for valuable discussions. This work has primarily been supported by a European Research Council (ERC) Advanced Investigator Grant (DYNALLO) and in part by the Swiss National Science Foundation through the National Center of Competence and Research (NCCR) MUST. RL acknowledges support from MRC (MR/K015931/1).

Supporting Information

Figures are included about the mass spectrum of the synthesized HP36Cys (Figure S1), TEM micrographs of the AuNPs and their size analysis (Figure S2), infrared spectrum of

PEG and tannic acid (Figure S3) and pump-probe analysis of the first and last 10 scans of the amide I recorded at 75 ps is . This information is available free of charge via the Internet at http://pubs.acs.org.

References

(1) Ferrari, M. Cancer nanotechnology: Opportunities and challenges. *Nat. Rev. Cancer* **2005**, *5*, 161-171.

(2) Kircher, M. F.; Mahmood, U.; King, R. S.; Weissleder, R.; Josephson, L. A Multimodal Nanoparticle for Preoperative Magnetic Resonance Imaging and Intraoperative Optical Brain Tumor Delineation. *Cancer Res.* **2003**, *63*, 8122-8125.

(3) Park, J. Liposome-based drug delivery in breast cancer treatment. *Breast Cancer Res.* **2002**, *4*, 95 - 99.

(4) Neuwelt, E. A.; Varallyay, P.; Bago, A. G.; Muldoon, L. L.; Nesbit, G.; Nixon, R. Imaging of iron oxide nanoparticles by MR and light microscopy in patients with malignant brain tumours. *Neuropathol. Appl. Neurobiol.* **2004**, *30*, 456-471.

(5) Li, K. C. P.; Pandit, S. D.; Guccione, S.; Bednarski, M. D. Molecular Imaging applications in nanomedicine. *Biomed. Microdevices* **2004**, *6*, 113-116.

(6) Kobayashi, T. Cancer hyperthermia using magnetic nanoparticles. *Biotechnol. Journal* **2011**, *6*, 1342-1347.

(7) Zhou, J.; Patel, T. R.; Sirianni, R. W.; Strohbehn, G.; Zheng, M.-Q.; Duong, N.; Schafbauer, T.; Huttner, A. J.; Huang, Y.; Carson, R. E.; Zhang, Y.; Sullivan, D. J.; Piepmeier, J. M.; Saltzman, W. M. Highly penetrative, drug-loaded nanocarriers improve treatment of glioblastoma. *Proc. Natl. Acad. Sci. U. S. A.* **2013**. *110*, 11751-11756.

(8) Hirsch, L. R.; Jackson, J. B.; Lee, A.; Halas, N. J.; West, J. A whole blood immunoassay using gold nanoshells. *Anal. Chem.* **2003**, *75*, 2377-2381.

(9) Kisak, E. T.; Coldren, B.; Evans, C. A.; Boyer, C.; Zasadzinski, J. A. The vesosome - A multicompartment drug delivery vehicle. *Curr. Med. Chem.* **2004**, *11*, 199-219.

(10) Paleos, C. M.; Tsiourvas, D.; Sideratou, Z.; Tziveleka, L. Acid- and salt-triggered multifunctional poly(propylene imine) dendrimer as a prospective drug delivery system. *Biomacromolecules* **2004**, *5*, 524-529.

(11) Wu, W.; Wieckowski, S.; Pastorin, G.; Benincasa, M.; Klumpp, C.; Briand, J. P.; Gennaro, R.; Prato, M.; Bianco, A.: Targeted delivery of amphotericin B to cells by using functionalized carbon nanotubes. *Angew. Chem. Int. Ed.* **2005**, *44*, 6358-62.

(12) Salem, A. K.; Searson, P. C.; Leong, K. W. Multifunctional nanorods for gene delivery. *Nat. Mater.* **2003**, *2*, 668-671.

(13) Dreaden, E. C.; Austin, L. A.; Mackey, M. A.; El-Sayed, M. A. Size matters: gold nanoparticles in targeted cancer drug delivery. *Ther. Deliv.* **2012**, *3*, 457-78.

(14) Dykman, L. A.; Khlebtsov, N. G. Gold Nanoparticles in Biology and Medicine: Recent Advances and Prospects. *Acta Naturae* **2011**, *3*, 34-55.

(15) Ghadiali, J. E.; Stevens, M. M. Enzyme-Responsive Nanoparticle Systems. *Adv. Mater.* **2008**, *20*, 4359-4363.

(16) Andresen, T. L.; Thompson, D. H.; Kaasgaard, T. Enzyme-triggered nanomedicine: Drug release strategies in cancer therapy (Invited Review). *Mol. Membr. Biol.* **2010**, *27*, 353-363.

(17) Hong, R.; Han, G.; Fernandez, J. M.; Kim, B. J.; Forbes, N. S.; Rotello, V. M. Glutathione-mediated delivery and release using monolayer protected nanoparticle carriers. *J. Am. Chem. Soc.* **2006**, *128*, 1078-1079.

(18) Kumar, D.; Meenan, B. J.; Dixon, D. Glutathione-mediated release of Bodipy (R) from PEG cofunctionalized gold nanoparticles. *Int. J. Nanomedicine* **2012**, *7*, 4007-4022.

(19) Lin, J.; Wang, S.; Huang, P.; Wang, Z.; Chen, S.; Niu, G.; Li, W.; He, J.; Cui, D.; Lu, G.; Chen, X.; Nie, Z. Photosensitizer-Loaded Gold Vesicles with Strong Plasmonic Coupling Effect for Imaging-Guided Photothermal/Photodynamic Therapy. *ACS Nano* **2013**, *7*, 5320-5329.

(20) O'Neal, D. P.; Hirsch, L. R.; Halas, N. J.; Payne, J. D.; West, J. L. Photo-thermal tumor ablation in mice using near infrared-absorbing nanoparticles. *Cancer Lett.* **2004**, *209*, 171-176.

(21) Hirsch, L. R.; Stafford, R. J.; Bankson, J. A.; Sershen, S. R.; Rivera, B.; Price, R. E.; Hazle, J. D.; Halas, N. J.; West, J. L. Nanoshell-mediated near-infrared thermal therapy of tumors under magnetic resonance guidance. *Proc. Natl. Acad. Sci. U. S. A.* **2003**, *100*, 13549-13554.

(22) Huang, X.; Qian, W.; El-Sayed, I. H.; El-Sayed, M. A. The potential use of the enhanced nonlinear properties of gold nanospheres in photothermal cancer therapy. *Lasers Surg. Med.* **2007**, *39*, 747-753.

(23) Hamad-Schifferli, K.; Schwartz, J. J.; Santos, A. T.; Zhang, S. G.; Jacobson, J. M. Remote electronic control of DNA hybridization through inductive coupling to an attached metal nanocrystal antenna. *Nature* **2002**, *415*, 152-155.

(24) Jain, P. K.; Qian, W.; El-Sayed, M. A. Ultrafast cooling of photoexcited electrons in gold nanoparticle-thiolated DNA conjugates involves the dissociation of the gold-thiol bond. *J. Am. Chem. Soc.* **2006**, *128*, 2426-2433.

(25) Ibrahimkutty, S.; Kim, J.; Cammarata, M.; Ewald, F.; Choi, J.; Ihee, H.; Plech, A. Ultrafast Structural Dynamics of the Photocleavage of Protein Hybrid Nanoparticles. *ACS Nano* **2011**, *5*, 3788-3794.

(26) Link, S.; Ei-Sayed, M. A. Optical properties and ultrafast dynamics of metallic nanocrystals. *Annu. Rev. Phys. Chem.* **2003**, *54*, 331-366.

(27) Hu, M.; Hartland, G. V. Heat dissipation for Au particles in aqueous solution: Relaxation time versus size. *J. Phys. Chem. B* **2002**, *106*, 7029-7033.

(28) Hartland, G. V. Measurements of the material properties of metal nanoparticles by time-resolved spectroscopy. *Phys. Chem. Chem. Phys.* **2004**, *6*, 5263-5274.

(29) Huang, X. H.; Jain, P. K.; El-Sayed, I. H.; El-Sayed, M. A. Determination of the minimum temperature required for selective photothermal destruction of cancer cells with the use of immunotargeted gold nanoparticles. *Photochem. Photobiol.* **2006**, *82*, 412-417.

(30) Hashimoto, S.; Werner, D.; Uwada, T. Studies on the interaction of pulsed lasers with plasmonic gold nanoparticles toward light manipulation, heat management, and nanofabrication. *J. Photoc. Photobio. C* **2012**, *13*, 28-54.

(31) Kubelka, J.; Hofrichter, J.; Eaton, W. A. The protein folding 'speed limit'. *Curr. Opin. Struct. Biol.* **2004**, *14*, 76-88.

(32) Carter, J. A.; Wang, Z. H.; Fujiwara, H.; Dlott, D. D. Ultrafast Excitation of Molecular Adsorbates on Flash-Heated Gold Surfaces. *J. Phys. Chem. A* **2009**, *113*, 12105-12114.

(33) Wang, Z.; Carter, J. A.; Lagutchev, A.; Koh, Y. K.; Seong, N. H.; Cahill, D. G.; Dlott, D. D. Ultrafast flash thermal conductance of molecular chains. *Science* **2007**, *317*, 787-90.

(34) Schade, M.; Moretto, A.; Donaldson, P. M.; Toniolo, C.; Hamm, P. Vibrational Energy Transport through a Capping Layer of Appropriately Designed Peptide Helices over Gold Nanoparticles. *Nano Lett.* **2010**, *10*, 3057-3061.

(35) Leitner, D. M. Energy flow in proteins. *Annu. Rev. Phys. Chem.* **2008**, *59*, 233-59.

(36) Tang, Y. F.; Grey, M. J.; McKnight, J.; Palmer, A. G.; Raleigh, D. P. Multistate folding of the villin headpiece domain. *J. Mol. Biol.* **2006**, *355*, 1066-1077.

(37) Bagchi, S.; Falvo, C.; Mukamel, S.; Hochstrasser, R. M. 2D-IR Experiments and Simulations of the Coupling between Amide-I and Ionizable Side Chains in Proteins: Application to the Villin Headpiece. *J. Phys. Chem. B* **2009**, *113*, 11260-11273.

(38) Brewer, S. H.; Vu, D. M.; Tang, Y. F.; Li, Y.; Franzen, S.; Raleigh, D. P.; Dyer, R. B. Effect of modulating unfolded state structure on the folding kinetics of the villin headpiece subdomain. *Proc. Natl. Acad. Sci. U. S. A.* **2005**, *102*, 16662-16667.

(39) Chiu, T. K.; Kubelka, J.; Herbst-Irmer, R.; Eaton, W. A.; Hofrichter, J.; Davies, D. R. High-resolution x-ray crystal structures of the villin headpiece subdomain, an ultrafast folding protein. *Proc. Natl. Acad. Sci. U. S. A.* **2005**, *102*, 7517-7522.

(40) Chung, J. K.; Thielges, M. C.; Fayer, M. D. Dynamics of the folded and unfolded villin headpiece (HP35) measured with ultrafast 2D IR vibrational echo spectroscopy. *Proc. Natl. Acad. Sci. U. S. A.* **2011**, *108*, 3578-3583.

(41) Wickstrom, L.; Okur, A.; Song, K.; Hornak, V.; Raleigh, D. P.; Simmerling, C. L. The unfolded state of the villin headpiece helical subdomain: Computational studies of the role of locally stabilized structure. *J. Mol. Biol.* **2006**, *360*, 1094-1107.

(42) Ripoll, D. R.; Vila, J. A.; Scheraga, H. A. Folding of the villin headpiece subdomain from random structures. analysis of the charge distribution as a function of pH. *J. Mol. Biol.* **2004**, *339*, 915-925.

(43) Kubelka, J.; Eaton, W. A.; Hofrichter, J. Experimental tests of villin subdomain folding simulations. *J. Mol. Biol.* **2003**, *329*, 625-630.

(44) Brewer, S. H.; Song, B. B.; Raleigh, D. P.; Dyer, R. B. Residue specific resolution of protein folding dynamics using isotope-edited infrared temperature jump spectroscopy. *Biochemistry* **2007**, *46*, 3279-3285.

(45) Brewer, S. H.; Vu, D. M.; Tang, Y.; Li, Y.; Franzen, S.; Raleigh, D. P.; Dyer, R. B. Effect of modulating unfolded state structure on the folding kinetics of the villin headpiece subdomain. *Proc. Natl. Acad. Sci. U. S. A.* **2005**, *102*, 16662-16667.

(46) Wang, L.; Skinner, J. L. Thermally Induced Protein Unfolding Probed by Isotope-Edited IR Spectroscopy. *J. Phys. Chem. B* **2012**, *116*, 9627-9634.

(47) Muhlpfordt, H. The Preparation of Colloidal Gold Particles Using Tannic-Acid as an Additional Reducing Agent. *Experientia* **1982**, *38*, 1127-1128.

(48) Hamm, P.; Kaindl, R. A.; Stenger, J. Noise suppression in femtosecond mid-infrared light sources. *Opt. Lett.* **2000**, *25*, 1798-800.

(49) Barth, A.; Zscherp, C. What vibrations tell us about proteins. *Q. Rev. Biophys.* **2002**, *35*, 369-430.

(50) Adato, R.; Yanik, A. A.; Amsden, J. J.; Kaplan, D. L.; Omenetto, F. G.; Hong, M. K.; Erramilli, S.; Altug, H. Ultra-sensitive vibrational spectroscopy of protein monolayers with plasmonic nanoantenna arrays. *Proc. Natl. Acad. Sci. U. S. A.* **2009**, *106*, 19227-19232.

(51) Donaldson, P. M.; Hamm, P. Gold Nanoparticle Capping Layers: Structure, Dynamics, and Surface Enhancement Measured Using 2D-IR Spectroscopy. *Angew. Chem. Int. Ed.* **2013**, *52*, 634-638.

(52) Shaw, C. P.; Middleton, D. A.; Volk, M.; Levy, R. Amyloid-derived peptide forms self-assembled monolayers on gold nanoparticle with a curvature-dependent beta-sheet structure. *ACS Nano* **2012**, *6*, 1416-26.

(53) Krpetic, Z.; Davidson, A. M.; Volk, M.; Levy, R.; Brust, M.; Cooper, D. L. High-Resolution Sizing of Monolayer-Protected Gold Clusters by Differential Centrifugal Sedimentation. *ACS Nano* **2013**, *7*, 8881-8890.

(54) Bauer, C.; Abid, J. P.; Girault, H. H. Size dependence investigations of hot electron cooling dynamics in metal/adsorbates nanoparticles. *Chem. Phys.* **2005**, *319*, 409-421.

(55) Aubin-Tam, M. E.; Hwang, W.; Hamad-Schifferli, K. Site-directed nanoparticle labeling of cytochrome c. *Proc. Natl. Acad. Sci. U. S. A.* **2009**, *106*, 4095-4100.

(56) Miura, Y.; Kimura, S.; Imanishi, Y.; Umemura, J. Oriented helical peptide layer on the carboxylate-terminated alkanethiol immobilized on a gold surface. *Langmuir* **1999**, *15*, 1155-1160.

(57) Sahoo, D.; Bhattacharya, P.; Patra, H. K.; Mandal, P.; Chakravorti, S. Gold nanoparticle induced conformational changes in heme protein. *J. Nanopart. Res.* **2011**, *13*, 6755-6760.

(58) Hamed, E.; Xu, T.; Keten, S. Poly(ethylene glycol) Conjugation Stabilizes the Secondary Structure of alpha-Helices by Reducing Peptide Solvent Accessible Surface Area. *Biomacromolecules* **2013**, *14*, 4053-60.

(59) Liu, X. O.; Atwater, M.; Wang, J. H.; Huo, Q. Extinction coefficient of gold nanoparticles with different sizes and different capping ligands. *Colloids and Surfaces B-Biointerfaces* **2007**, *58*, 3-7.

(60) Botan, V.; Backus, E. H. G.; Pfister, R.; Moretto, A.; Crisma, M.; Toniolo, C.; Nguyen, P. H.; Stock, G.; Hamm, P. Energy transport in peptide helices. *Proc. Natl. Acad. Sci. U. S. A.* **2007**, *104*, 12749-12754.

(61) Helbing, J.; Devereux, M.; Nienhaus, K.; Nienhaus, G. U.; Hamm, P.; Meuwly, M. Temperature dependence of the heat diffusivity of proteins. *J. Phys. Chem. A* **2012**, *116*, 2620-8.

(62) Ge, Z. B.; Kang, Y. J.; Taton, T. A.; Braun, P. V.; Cahill, D. G. Thermal transport in Au-core polymer-shell nanoparticles. *Nano Lett.* **2005**, *5*, 531-535.

(63) Amunson, K. E.; Kubelka, J. On the temperature dependence of amide I frequencies of peptides in solution. *J. Phys. Chem. B* **2007**, *111*, 9993-9998.

(64) Volk, M.; Kholodenko, Y.; Lu, H. S. M.; Gooding, E. A.; DeGrado, W. F.; Hochstrasser, R. M. Peptide conformational dynamics and vibrational stark effects following photoinitiated disulfide cleavage. *J. Phys. Chem. B* **1997**, *101*, 8607-8616.

(65) Cleland, J. L.; Hedgepeth, C.; Wang, D. I. C. Polyethylene-Glycol Enhanced Refolding of Bovine Carbonic Anhydrase-B - Reaction Stoichiometry and Refolding Model. *J. Biol. Chem.* **1992**, *267*, 13327-13334.

(66) Tokuriki, N.; Kinjo, M.; Negi, S.; Hoshino, M.; Goto, Y.; Urabe, I.; Yomo, T. Protein folding by the effects of macromolecular crowding. *Protein Sci.* **2004**, *13*, 125-133.

(67) El-Sayed, I. H.; Huang, X. H.; El-Sayed, M. A. Selective laser photo-thermal therapy of epithelial carcinoma using anti-EGFR antibody conjugated gold nanoparticles. *Cancer Lett.* **2006**, *239*, 129-135.

TOC Graphics

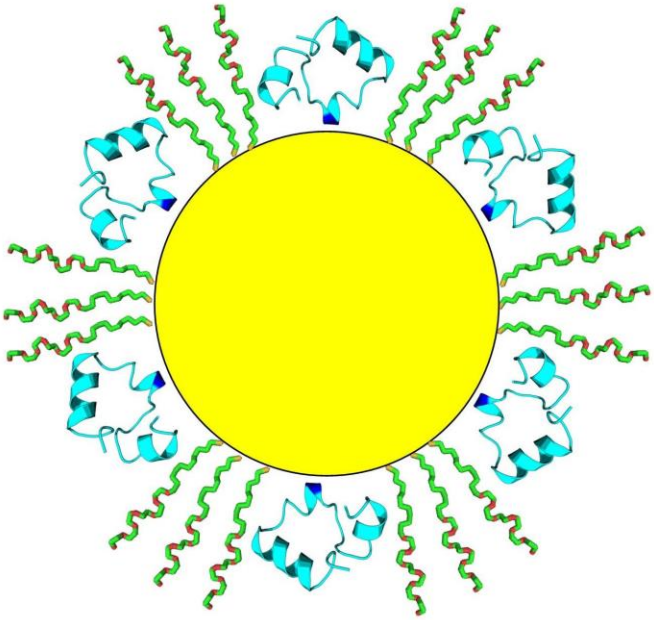

A small protein (villin headpiece) bound to AuNPs is heated to dramatic temperatures (≈1000 K) through the excitation of the AuNPs, but nevertheless remains folded since the heat jump lives for a few nanoseconds only.